Food Chemistry: X 24 (2024) 101942

Contents lists available at ScienceDirect

Food Chemistry: X

journal homepage: www.sciencedirect.com/journal/food-chemistry-x

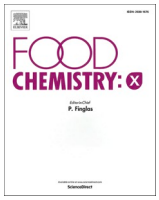

# Insight into characteristics in rice starch under heat- moisture treatment: Focus on the structure of amylose/amylopectin

Weijie Qi, Siying Kong, Xiaoqiang Li, Zeyu Peng, Lina Sun, Zhaohua Wang, Jianjun Cheng *

*College of Food Science, Northeast Agricultural University, Harbin 150030, China*

ARTICLE INFO

*Keywords:*
Starch
Heat-moisture treatment
Structure
Physiochemical characteristics
Digestive characteristics

ABSTRACT

Heat-moisture treatment (HMT) could improve the structure and physicochemical characteristics of rice starch, the structural changes of amylose and amylopectin needed to be further investigated. Hence, the starch, amylose and amylopectin were modified by HMT with different moisture contents (MC). As MC increased, starch granules became irregular, amylose appeared molten while amylopectin was less damaged. The crystal structure of starch was disrupted by HMT. The increase in the double helix structure of amylose exhibited more drastic tendency towards molecular rearrangement than amylopectin did. In addition, the reduced proportion of amylopectin A chain could affect the rearrangement of amylose. The solubility and pasting temperature improved, but the enthalpy decreased. Moderate MC (20 %, 25 %) could enhance the viscosity and dynamic viscoelasticity. HMT promoted the conversion of RDS to RS, which was significantly increased by 85.26 % at HMT-40 %. These findings contributed to a better understanding of the mechanisms by which HMT affected starch.

## 1. Introduction

Rice serves as a primary food source, fulfilling the majority of the population's energy and nutritional requirements. Starch constitutes approximately 75 %–82 % of the total composition of rice grains. This starch is predominantly composed of polysaccharides, with α-D-glucopyranose serving as the fundamental constituent unit. The composition of starch is characterized by two distinct types of glucans: amylose and amylopectin. Amylose is characterized by its long, linear polymer structure linked by α-(1, 4) bonds, whereas amylopectin exhibits "cluster" polymer configuration, interconnected by both α-(1, 4) and α-(1, 6) linkages. Furthermore, starch possesses various multilayered structures, including crystalline and amorphous lamellae, growth rings comprising alternating amorphous and crystalline layers, and granular morphology (Tao, Li, Yu, Gilbert, & Li, 2019). The different structures lead to their inconsistent function, which are crucial for the processing and application for starchy foods.

Natural starch has limited its development in industrial applications owing to its insolubility, ease of retrogradation, and ease of digestion. Consequently, physical, chemical, and enzymatic modifications of starch have emerged as areas of intense research focus. These modification techniques have yielded improvements in various aspects, including structural alterations of granules, enhanced swelling power (SP), increased solubility, modified rheological characteristics, and improved digestive and thermal stability. In the context of food manufacturing, physical modification is preferentially employed due to food safety considerations. Current physical modification methodologies primarily encompass annealing, microwave treatment, high hydrostatic pressure, and freeze-thaw processes. Heat-moisture treatment (HMT) has garnered particular attention due to its advantages of low cost, flexible heat source options, and absence of chemical residues, rendering it a simple yet effective modification technique. HMT is typically conducted under conditions where MC does not exceed 35 % at elevated temperatures ranging from 100 °C to 120 °C (Wang, Li, Liu, & Zheng, 2022). During the HMT process, starch undergoes segmental movements, resulting in the transformation of amorphous structural domains from a glassy state to a more flexible configuration (Wang et al., 2018). Additionally, HMT induces the disruption of certain crystal structures and the separation of double helix formations while simultaneously promoting the rearrangement of starch chains (Schafranski, Ito, & Lacerda, 2021).

The impact of HMT on starch has been extensively investigated, with research primarily focusing on moisture content (MC), starch source, temperature, duration, heating methodology, and amylose content. The amylose content has been demonstrated to significantly influence starch rearrangement behavior, thereby affecting its structure and

* Corresponding author.
*E-mail address:* jjcheng@neau.edu.cn (J. Cheng).

https://doi.org/10.1016/j.fochx.2024.101942
Received 19 September 2024; Received in revised form 28 October 2024; Accepted 28 October 2024
Available online 30 October 2024

functionality (Kumar et al., 2023). Moreover, HMT-treated high-amylose starches have exhibited enhanced enzyme resistance compared to their natural counterparts, suggesting the potential for increasing resistant starch content in starch-based products (Wang, Zhang, Chen, & Li, 2016). As previously discussed, the linear starch content exerts a considerable influence on both starch structure and food processing modifications. Guo et al. (2020) employed annealing treatment to modify amylose and amylopectin, revealing that amylose exhibited greater sensitivity to the process. Zhong, Tian, Liu, Ding, and Blennow (2021) demonstrated that microwave treatment of amylose and amylopectin granules resulted in distinctly different reorganization patterns, with a notable reduction in amylose crystallinity. These findings support the hypothesis that amylose is more susceptible to HMT, potentially leading to more pronounced structural alterations. However, the molecular mechanisms underlying HMT-induced changes have been insufficiently analyzed from the perspective of amylose versus amylopectin. Further investigation is required to elucidate the structural changes in starch, amylose, and amylopectin and to establish the correlations between these changes and their functional characteristics. Additionally, the rearrangement and physicochemical properties of starch molecules, as well as the mechanisms of alteration, necessitate further elucidation.

Hence, we extracted and isolated and purified the starch, amylose and amylopectin. The structures variations were mutually verified by Scanning electron microscope (SEM), X-ray diffraction (XRD), Fourier transform infrared (FTIR) spectra, Raman spectra and size exclusion chromatography (SEC) under HMT treatment conditions with different MC (0, 20 %, 25 %, 30 % and 35 %). Further studies on the physicochemical characteristics of starch were carried out to elucidate the mechanism of the structure-property relationship. The findings of the present study enable us to better understand the structure of starch, both amylose and amylopectin, in relation to the characteristics under HMT treatment.

## 2. Materials and methods

### 2.1. Materials

Rice (cultivar “Suijing18”, CNA20131182.9) was obtained from the Heilongjiang Academy of Agricultural Sciences. Rice starch was extracted in the laboratory, exhibiting a starch purity of 92.78 %, an amylose content of 12.20 %, a protein content of 0.41 %, and a lipid content of 0.25 %. Both amylose and amylopectin were extracted in the laboratory. Standard amylose (A8160) and amylopectin (A8150) were procured from Solaibao Co., Ltd. (Beijing, China). The α-amylase (40 U/mg, A8750–250) and amyloglucosidase (100 U/g, T8500) were also supplied by Solaibao Co., Ltd. (Beijing, China). All other reagents utilized were of analytical grade.

### 2.2. Isolation of rice starch

The isolation process was based on the method described by Chen et al. (2019), and with appropriate modifications. Rice was thoroughly soaked in distilled water (DI water), subsequently milled in a wall breaker for 2 min, and filtered through a 200-mesh sieve. The filtrate was then mixed with 1 L of NaOH (0.05 mol/L) under constant stirring. Centrifugation at 5000*g* for 15 min was employed to remove the supernatant and protein layer. This process was repeated until no further protein was observed. The resulting precipitate was dissolved in water, and its pH was adjusted to 7.0 using HCl (0.1 mol/L). Non-starch sugars and lipids were eliminated by dissolving the precipitate in a mixture of ethanol and ether (4:1, *v*/v) and stirring for 3 h. The suspension was then centrifuged (3000 *g*, 15 min), and the precipitate was freeze-dried for 12 h. The obtained starch was ground, sieved, and stored under dry conditions.

### 2.3. Separation and purification of amylose and amylopectin

The separation method was based on the principle that amylose forms a complex with n-butanol, allowing for its precipitation (Guo et al., 2020). Amylose and amylopectin were separated under centrifugal conditions, followed by the separation of amylose-n-butanol complexes.

#### 2.3.1. Crude extraction

Starch (50 g) was initially dispersed with a small amount of anhydrous ethanol, after which 700 mL of NaOH was added. The solution was heated and stirred in a boiling water bath for 15 min until no precipitation was observed, then cooled. Following centrifugation (9000 *g*, 10 min), the solution was neutralized with HCl. A mixture of n-butanol and isoamyl alcohol (3:1, *v*/v, 200 mL) was added and stirred in a boiling water bath for 10 min. After cooling, the solution was refrigerated (4 °C, 12 h) and subsequently centrifuged (9000 *g*, 10 min). The resulting precipitate was identified as crude amylose, while the supernatant contained crude amylopectin.

#### 2.3.2. Purification of amylose

The crude amylose precipitate was transferred into 400 mL of saturated aqueous n-butanol solution and heated in a water bath until complete dissolution. The solution was then cooled and refrigerated (4 °C, 12 h). After centrifugation (9000 *g*, 10 min), the precipitate was filtered through a sand core funnel. This process was repeated several times, and the precipitates were collected. The collected precipitate was rinsed three times by immersion in anhydrous ethanol. Purified amylose was obtained through freeze-drying for 12 h. Finally, the amylose was ground, sieved through a 100-mesh sieve, dried, and stored for further use.

#### 2.3.3. Purification of amylopectin

The supernatant obtained previously was placed in a dispensing funnel until the solution separated into three distinct layers. The lowest layer, exhibiting a latex-like consistency, was extracted. This latex-like liquid was subsequently combined with 80 mL of n-butanol-isoamyl alcohol mixture (1:1, *v*/v). The resulting solution was subjected to heating and stirring for 15 min under boiling water bath conditions, followed by cooling and refrigeration at 4 °C for 24 h. The cooled mixture was then centrifuged at 9000 *g* for 10 min. Amylopectin pre-precipitation was initiated by adding twice the volume of anhydrous ethanol to the supernatant. This process was repeated several times, and the precipitates were collected. The collected precipitate underwent three rinses with anhydrous ethanol and was subsequently freeze-dried for 12 h to obtain purified amylopectin. Finally, the purified amylopectin was milled, passed through a 100-mesh sieve, dried, and stored for future use.

#### 2.3.4. Assay of purity

The purity of the extracted amylose and amylopectin was determined using iodine colorimetry, as described by Guo et al. (Guo et al., 2020). A 0.1 g sample of either amylose or amylopectin was dispersed in 10 mL of NaOH solution. Deionized (DI) water was added, and the mixture was heated in a boiling water bath for 10 min, followed by rapid cooling. A 5 mL aliquot of this mixture was diluted with 25 mL of DI water, and the pH was adjusted to 3 using 0.1 mol/L HCl. Subsequently, 1 mL of iodine solution was added, and the volume was adjusted to the graduated line. The absorbance spectrum was measured using a spectrophotometer over the wavelength range of 400–800 nm. Standard curves were established using various ratios of amylose and amylopectin standard solutions, based on the wavelength of the absorption peak (Fig. S1d-f). The purity of amylose and amylopectin was determined to be 93.05 % ± 0.17 % and 90.12 % ± 0.13 %, respectively. These findings were further corroborated by visual color rendering upon addition of iodine solution, as illustrated in Fig. S1g.

### 2.4. HMT

Starch, amylose, and amylopectin samples (10 g each) were subjected to MC determination. A calculated amount of water was added to achieve the desired MC in the starch (20 %, 25 %, 30 %, and 35 %). The samples were then sealed in bags and stored at 4 °C for 24 h. To ensure homogeneity, manual stirring was performed every 2 h during this period. Subsequently, the samples were transferred to sealed glass jars and heated in an oven at 110 °C for 3 h. After cooling, the processed samples were milled using a ceramic mortar, and the resulting powder was sieved through a 100-mesh sieve. Untreated starch served as a control, while the modified starch samples were designated as HMT-20 %, HMT-25 %, HMT-30 %, and HMT-35 % (Wang et al., 2022).

### 2.5. Microstructural identification of amylose and amylopectin

Amylose and amylopectin samples were individually applied to microscope slides using an inoculating needle. An appropriate amount of DI water was added to facilitate dispersion. The slides were maintained at room temperature until complete water evaporation occurred, followed by staining with iodine solution. Microscopic observations were conducted using a Light microscopy system (Olympus Co., Ltd., Japan) at magnifications of ×200 and ×400 (Wang et al., 2022).

### 2.6. Structural characteristics

#### 2.6.1. Granular feature

The morphological characteristics of starch, amylose, and amylopectin were examined using an S-3400 N scanning electron microscope (Hitachi Co., Ltd., Japan). Micrographs were captured at magnifications of ×3000 and ×300, with an accelerating voltage of 3 kV (Gong et al., 2017).

#### 2.6.2. The X-ray diffraction

The crystalline structure of starch, amylose, and amylopectin was analyzed using X-ray diffractometry (Malvern Panalytical, Netherlands). Diffraction patterns were recorded over a 2θ angle range of 4° to 40°, with a step size of 0.05° and a scanning speed of 2°/min, following the method outlined by Rubio (Lopez-Rubio, Flanagan, Gilbert, & Gidley, 2010). The relative crystallinity (RC) was subsequently calculated using JADE 5.0 software.

#### 2.6.3. The fourier transform infrared spectra

Based on the analysis of the short-range structure of starch by Wang et al. (2022), with minor modifications. In brief, all samples were examined by iS10 FTIR spectrometer (Thermo Fisher Scientific, USA) in the range 4000–400 $cm^{-1}$. After obtaining the plots, they were processed with Omnic 8.0 software. The deconvolution of the characteristic peaks in the 1200–900 $cm^{-1}$ section was performed. The half-width peak was 25 cm and the enhancement factor was 2.0. The intensity of the characteristic peaks at 995 $cm^{-1}$, 1022 $cm^{-1}$ and 1047 $cm^{-1}$ was compared. Among them, the degree of order (DO) was the ratio of peak heights at 1047 $cm^{-1}$ and 1022 $cm^{-1}$. Degree of double helix (DD) was the ratio at 995 $cm^{-1}$ and 1022 $cm^{-1}$.

#### 2.6.4. The Raman spectra

Short-range structural analysis of starch samples was conducted using a laser confocal Raman spectrometer (Thermo Fisher Scientific, USA). Spectra were acquired over the range of 3200 $cm^{-1}$ to 100 $cm^{-1}$, with a laser power of 100 %, a laser wavelength of 532 nm, and a spectral resolution of 7 $cm^{-1}$. The full width at half maximum (FWHM) of the peak at 480 $cm^{-1}$ was determined using Wire 2.0 software (Lu, Tian, & Ma, 2023).

#### 2.6.5. Size-exclusion chromatography

The absolute molecular weights of amylose and amylopectin were determined using a gel chromatography-oscillometric-multiangle laser scattering system. This system comprised a U3000 liquid phase system (Thermo, USA), an oscillometric detector Opatilab T-rEX (Wyatt technology, CA, USA), and a laser scatterer DAWN HELEOS (Wyatt technology, CA, USA). Appropriate gel chromatography columns (Ohpak SB-805 HQ, Ohpak SB-804 HQ, Ohpak SB803 HQ, USA) were selected for the assay. The analysis was conducted with a flow rate of 0.3 mL/min, a dn/dc value of 0.07 mL/g, and an isocratic elution time of 120 min. The SEC spectra exhibited single peaks, indicating high purity of the samples. The absolute molecular weights of amylose and amylopectin were determined to be 18,288.47 kDa and 88,921.15 kDa, respectively (Fig. 1c).

For the analysis of starch molecules, a U3000 SEC system (Thermo, USA) equipped with a differential detector (Wyatt technology, CA, USA) was employed to obtain the molecular weight size distribution and chain length distribution (CLD). Gel exclusion chromatography columns (Ohpak SB-805 HQ, Ohpak SB803 HQ, USA) with appropriate molecular weight ranges were utilized based on the characteristics of the starch molecules. Standards were obtained from APSC, and the mobile phases consisted of LiBr and DMSO. The flow rate was maintained at 0.3 mL/min with an elution gradient of 120 min. It should be noted that the amylopectin composition in the whole-molecule distribution was not reliably quantifiable due to an unavoidable shear fracture during SEC analysis. The degree of shear fracture was dependent on the SEC conditions, including the state of the column at the time of the run. However, the composition of amylose was not affected by this issue. As previously mentioned, the corresponding quantities of amylopectin were not accurate but could be used to indicate trends under the same setup conditions on the same machine (Tao et al., 2019). The hydrodynamic radius (Rh) could be transformed into the degree of polymerization (DP, X) using the Mark-Houwink equation, providing further insights into the structural characteristics of the starch molecules.

### 2.7. Physicochemical properties

#### 2.7.1. Solubility and SP

The solubility and swelling power of starch samples were determined using the following methodology. A measured quantity of starch was dispersed in 50 mL of DI water. The resulting suspensions were stirred at 25 °C and 100 °C for 30 min, respectively. Subsequently, the samples were centrifuged at 3000 *g* for 15 min. The mass of the precipitate was recorded as $m_1$. The supernatant was subjected to drying at 105 °C until a constant weight was achieved, and this value was recorded as $m_2$. The solubility and SP were calculated using the following eqs. (Q. Wang et al., 2022).

$$Solubility(\%) = 100 \times m_2/0.3 \quad (1)$$

$$SP(g/g) = m_1/[0.3 \times (1 - solubility/100)] \quad (2)$$

#### 2.7.2. Pasting properties

The pasting characteristics of starch samples were analyzed using a Rapid Visco Analyzer (RVA) (Perkone Instruments, Hangzhou, China). Based on the MC, an appropriate volume of water was added to achieve a final concentration of 2 % (*w/v*). The starch suspension was initially equilibrated at 50 °C for 1 min, followed by heating to 95 °C at a rate of 6 °C/min. The temperature was maintained at 95 °C for 5 min. Subsequently, the sample was cooled to 50 °C at a rate of 6 °C/min and held at this temperature for 2 min (Zhong et al., 2023). The following parameters were obtained from the RVA profile: peak viscosity (PV), trough viscosity (TV), breakdown (BD), setback viscosity (SV), final viscosity (FV), and setback (SB).

#### 2.7.3. Differential scanning calorimetry

Thermal properties of starch samples were evaluated using a differential scanning calorimeter (Mettler Toledo Instruments Ltd., Shanghai,

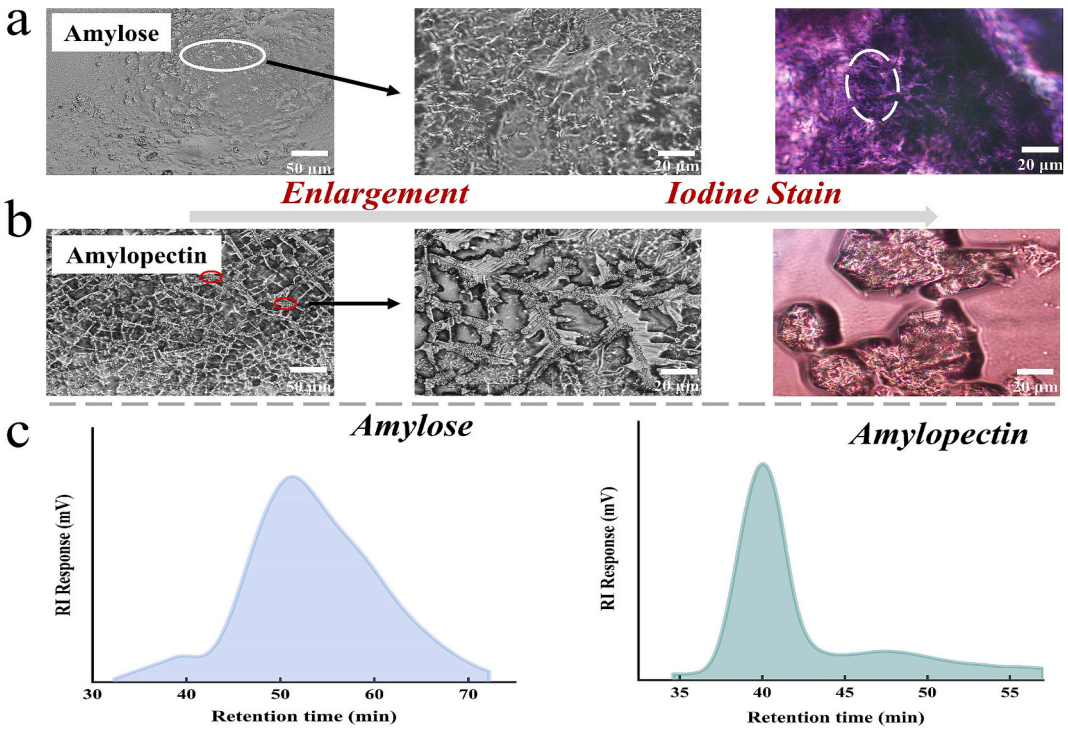


**Fig. 1.** Identification of amylose and amylopectin. The light microstructure (a, b) and size exclusion chromatography spectra (c) of extracted amylose and amylopectin.

China). A 3 mg starch sample was hermetically sealed in a crucible containing 9 μL of DI water. The sample was then heated from 30 °C to 100 °C at a rate of 10 °C/min (Zheng et al., 2021).

#### 2.7.4. Rheological properties

Rheological properties of starch samples were assessed using a Haake Mars 40-rheometer (Thermo Fisher Scientific, USA). Starch paste obtained from the RVA analysis was used for this purpose. A flat plate measuring system with a 35 mm diameter was employed for the rheological measurements. The apparent viscosity of the starch paste was determined as a function of shear rate, ranging from 0.1 to 100 $s^{-1}$. Additionally, frequency sweep experiments were conducted over a range of 0.1–10 Hz at a constant strain value of 1 %. To prevent water evaporation during the experiments, the edges of the samples were sealed with silicone oil (Ang, Goh, Lim, & Matia-Merino, 2021).

### 2.8. Simulated in vitro digestion

The starch digestion characteristics were evaluated using a modified method described by Yin et al. (2021). A 200 mg sample of starch (dry weight) was introduced into a beaker containing 10 mL of sodium acetate buffer. The mixture was equilibrated at 37 °C for 30 min, followed by the addition of α-amylase and amyloglucosidase. Glucose release was monitored at 20-min intervals. At each sampling point, 0.5 mL of digest was extracted and mixed with 3.5 mL of anhydrous ethanol to deactivate the enzymes. The resulting mixture was centrifuged at 4000 *g* for 15 min. The glucose concentration in the supernatant was quantified using a glucose oxidase-peroxidase (GOPOD) kit (BC2500). The rapidly digested starch (RDS), slowly digested starch (SDS), and resistant starch (RS) contents were calculated using the following equations:

$$RDS = \frac{(G_{20} - G_0) \times 0.9}{TS} \times 100 \quad (3)$$

$$SDS = \frac{(G_{120} - G_{20}) \times 0.9}{TS} \times 100 \quad (4)$$

$$RS = \frac{TS - RDS - SDS}{TS} \times 100 \quad (5)$$

where $G_0$, $G_{20}$ and $G_{120}$ represented the glucose content at 0, 20 and 120 min, respectively. TS represented the total starch mass in the in vitro digestive system. 0.9 was the conversion factor between glucose and starch.

### 2.9. Statistical analysis

Analysis of variance (ANOVA) was employed to compare differences between treatments. Duncan's multiple range test was conducted using SPSS 16.0 software. Statistical significance was established at $p < 0.05$, and correlation analysis was performed using the Pearson correlation test.

## 3. Results and discussion

### 3.1. Microstructural identification of amylose and amylopectin

The surface morphology of amylose and amylopectin was characterized using light microscopy. As illustrated in Fig. 1a and b, amylose exhibited an aggregated granular state, while amylopectin displayed an "urban network" distribution at 200× magnification. Upon closer examination at 400× magnification, significant structural differences between amylose and amylopectin were observed. Amylose presented as irregular clusters of curved, randomly arranged threads, whereas amylopectin resembled the "bundle cluster" model proposed by previous researchers, with a backbone chain featuring numerous branches (Bertoft, Koch, & Åman, 2016; Hizukuri, 1986; Vamadevan & Bertoft, 2015). Iodine staining of the two starch fractions revealed distinct colorimetric differences: amylose stained dark purple, while amylopectin appeared light purple. The observed agglomeration of both starch fractions was attributed to water-absorbing polymerization. Although the stained samples appeared somewhat blurred, original structural features could still be discerned in the free portions of the samples. In

conclusion, the combined characterization techniques of microstructural analysis, iodine colorimetry, and SEC confirmed the suitability of the derived raw materials for subsequent experiments.

### 3.2. Microscopic morphology

The microstructure of starch subjected to various MC and high-temperature conditions is illustrated in Fig. 2 (a1-a5). Prior to treatment, the starch granules exhibited irregular polygonal shapes, with small particles aggregated. No significant alterations were observed on the starch granule surfaces at 20 % and 25 % MC. This observation aligns with a previous study by Wang et al. (2022), who reported that the surface of blue wheat starch treated with HMT (15 % and 20 %, 100 °C) generally remained smooth. At 30 % MC, some starch granules displayed edge deformation, and granule aggregation became more pronounced (yellow arrow). In starch treated with HMT-35 %, irregular fragments overflowed, some granules were pasted, and their morphology became increasingly difficult to distinguish from the original structure. This phenomenon may be attributed to the gradual activation of water molecules during treatment, causing granule swelling and pressure-induced damage (Tan X et al., 2017). Therefore, compared to the control, with the increasing MC (especially HMT-30 % and HMT-35 %), the starch granules swelled significantly, the particle size increased, and the morphological changed and the degree of aggregation were beyond expectation. It was hypothesized that the starch spillage could act as binder to keep the starch granules together after HMT treatment. The underlying cause of this morphological change could be attributed to the partial gelatinization of starch during the HMT process, leading to swelling, rearrangement and surface roughness of starch granules (Yuxiu Zhong et al., 2023). Also, similar results were observed in plantain starch by Watcharatewinkul, Puttanlek, Rungsardthong, and Uttapap (2009).

The morphology of amylose and amylopectin is depicted in Fig. 2 (b1-b5) and (c1-c5), respectively. Both amylose and amylopectin particles exhibited irregular or polygonal shapes, with a rock-like, flattened appearance and a more pronounced laminar structure. Amylose granules displayed a rougher surface compared to amylopectin, consistent with the morphology of amylose and amylopectin isolated from sweet potatoes, as observed by Wang et al. (2022). It was evident that the morphology of amylose was more significantly affected by HMT treatment. As MC increased, amylose granules appeared to be fractured and melted, exhibiting irregular shapes and an increased number of cavities. In contrast, the changes in amylopectin were less dramatic, with surface cracks appearing on the granules but no signs of melting. This observation represents a novel finding not previously reported in the literature.

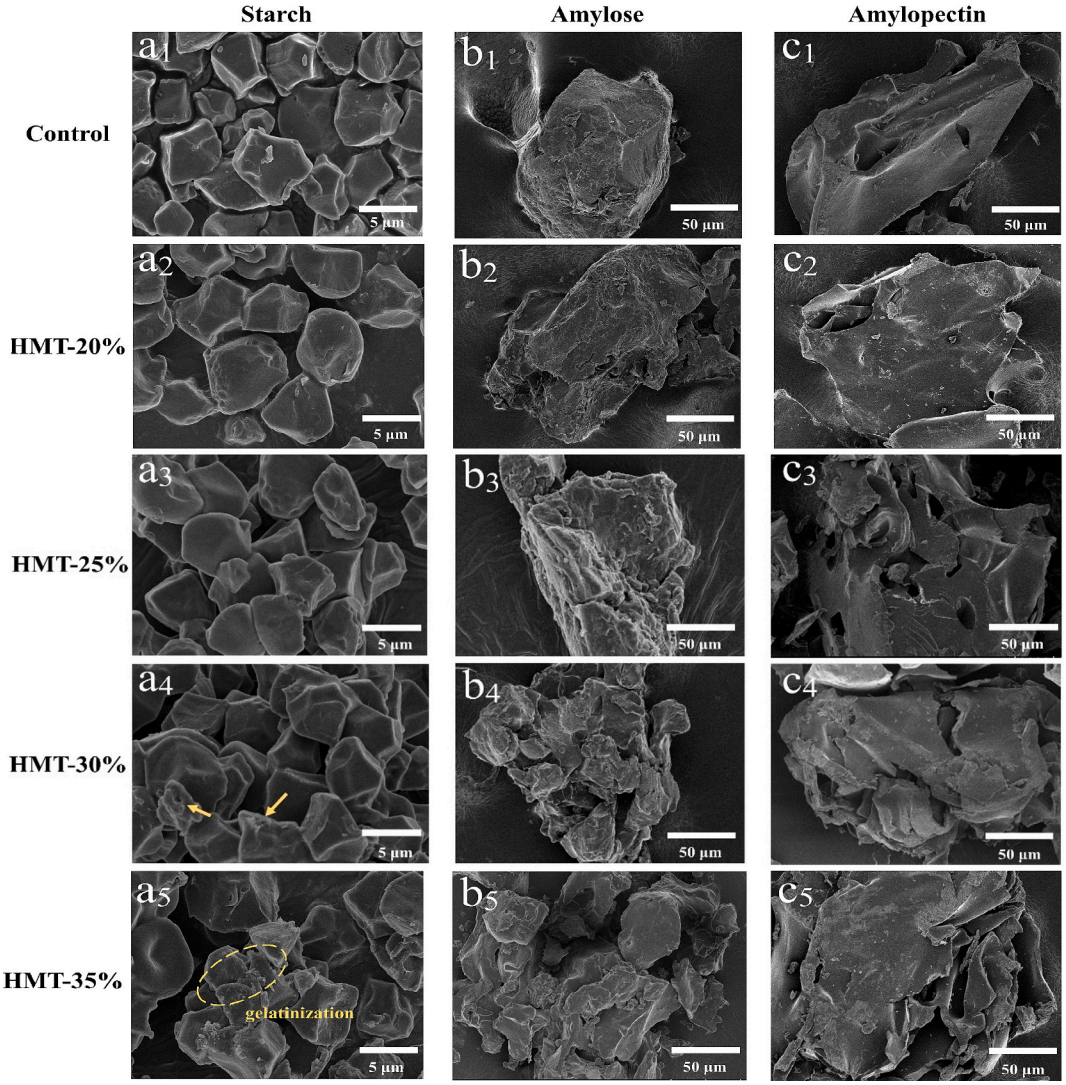


**Fig. 2.** SEM images of HMT-modified starch, amylose and amylopectin. Note: ($a_1$-$a_5$) starch, ($b_1$-$b_5$) amylose and ($c_1$-$c_5$) amylopectin.

### 3.3. Crystalline structure

The XRD is employed to examine dense helical structures form crystalline arrays in starch. From the XRD diagram of Fig. 3a, it could be noticed that the starch appeared distinct diffraction peaks at 14.68°, 17.08°, 17.78° and 22.57°, representing A-type crystalline polycrystals. After HMT modification, the peak positions did not show obvious shifts and all starch samples still showed A-type crystals. The peak at 19.80° showed no change, indicating that it was difficult to change the original V-type crystal at HMT conditions. It was noteworthy that the peak intensities decreased gradually with increasing MC. The diffraction peak intensities of HMT-35 % and HMT-40 % exhibited larger decreases, implying that the crystallographic surfaces were reduced in starch.

The amylose and amylopectin displayed different diffraction peaks. Amylose appeared diffraction peaks at 12.83°, 16.94°, 19.59° and 22.34°, which were different from the peak of starch (Fig. 3b). In contrast, amylopectin only showed diffraction peaks at 19.47° (Fig. 3c). From the crystal structure, amylose was obviously affected by HMT. The disappearance of the diffraction peak at 12.83° reflected the degradation of amylose, which was also confirmed in previous study (Zhong et al., 2021). Interestingly, the V-type structure at 19.59° remained, demonstrating that it was the main factor in maintaining the V-type crystal. The peaks at 16.94° and 22.45° did not change significantly, which was consistent with the change of starch. The X-ray curves of amylopectin with HMT exhibited little change in the peak at 19.47°, which revealed that the effect of HMT on the amylopectin was smaller and more different from that of the amylose. Based on the diffraction peak changes, it seemed reasonable to assume that the amylose had greater influence on the starch structure during HMT treatment.

The RC, which reflect variations in peak intensity, are presented in Fig. 3d, e and f for starch, amylose, and amylopectin, respectively. The RC of HMT-20 % starch increased initially but showed a gradual decreasing trend with increasing MC. This phenomenon can be attributed to the formation of double helix structures at low MC, where disordered chains in the amorphous region combine with amylopectin to complement crystalline defects (Wang et al., 2022). As MC increased, glycosidic bond breakage in the crystalline region hindered starch helical structure extension, while hydrogen bonding disruption at the $C_6$ position further contributed to this effect (Sun et al., 2021). These factors impeded starch chain aggregation into larger cocrystals, resulting in decreased crystal size and, consequently, reduced RC. Correspondingly, amylopectin RC initially decreased with increasing MC relative to the control, followed by a slight increase. This trend may be explained by the degradation of amylopectin-type glucans into smaller, more flexible molecules. The conversion of thermal energy into kinetic energy could enhance the activity of these degraded molecules, promoting double helix molecular reorganization. Conversely, amylose RC consistently decreased with increasing water content. Unlike amylopectin, amylose molecules were unable to form ordered structures and exhibited greater mobility. As MC increased, amylose degradation produced short-chain molecules, potentially inhibiting the formation of large crystal structures (Zhong et al., 2021). The destruction of amylose by HMT was more pronounced compared to amylopectin. At high MC, starch RC was reduced relative to the control, supporting the hypothesis that short chains resulting from amylopectin degradation hindered amylose rearrangement. Consequently, under HMT conditions, amylose molecules demonstrated a more pronounced tendency towards molecular rearrangement.

### 3.4. Short-range crystalline structure

#### 3.4.1. FTIR spectra

FTIR spectroscopy was employed to measure the ordered helical structure within or outside the crystal array (short-range crystalline structure) (Guo et al., 2020). As evidenced in Fig. 4a, no new absorption bands were observed in the spectra of HMT-treated starch samples compared to the control. This observation indicates that HMT altered the arrangement of starch chains without modifying the chemical bond

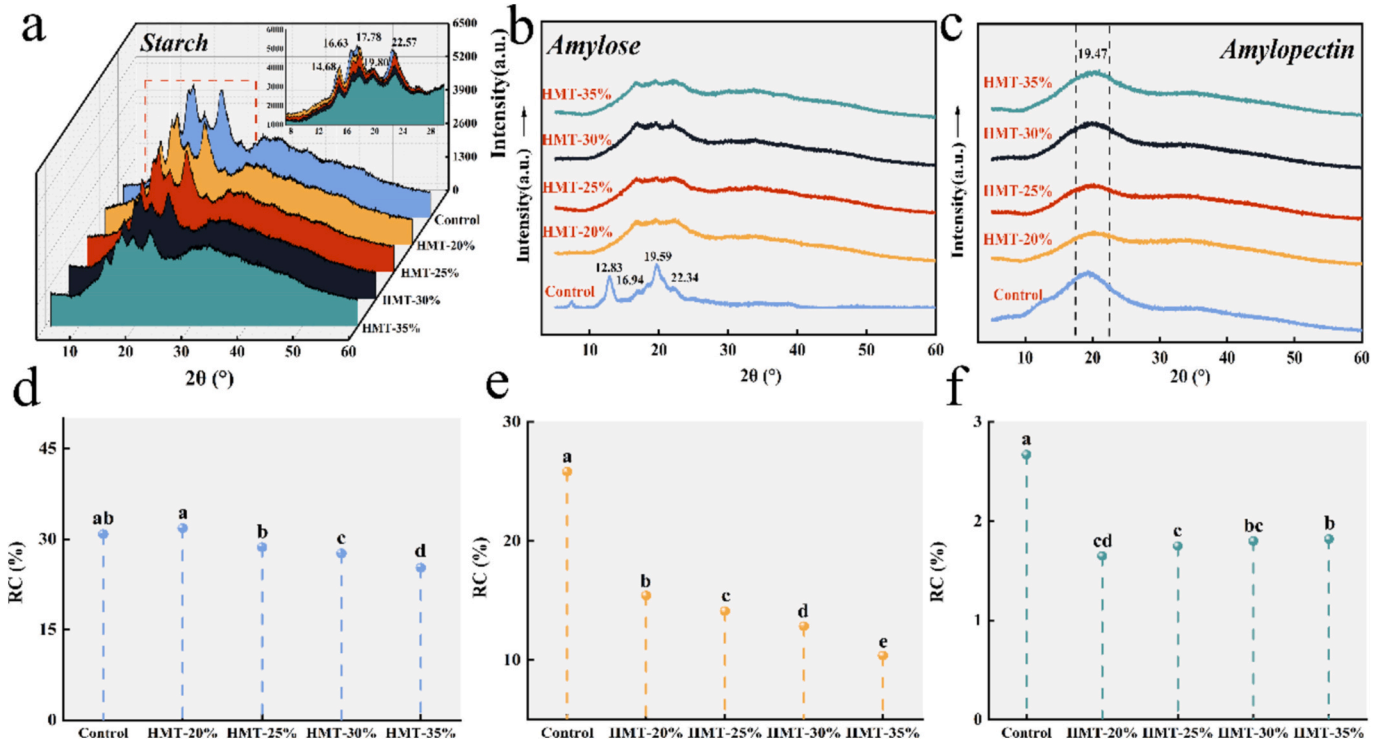


**Fig. 3.** XRD diagram of starch, amylose and amylopectin modified by HMT. (a-c) XRD diagram of starch, amylose and amylopectin. (d-f) the relative crystallinity (RC) of starch, amylose and amylopectin. Different lowercase letters (a-e) indicate significant differences ($p<0.05$) in the mean values within the same parameter group.

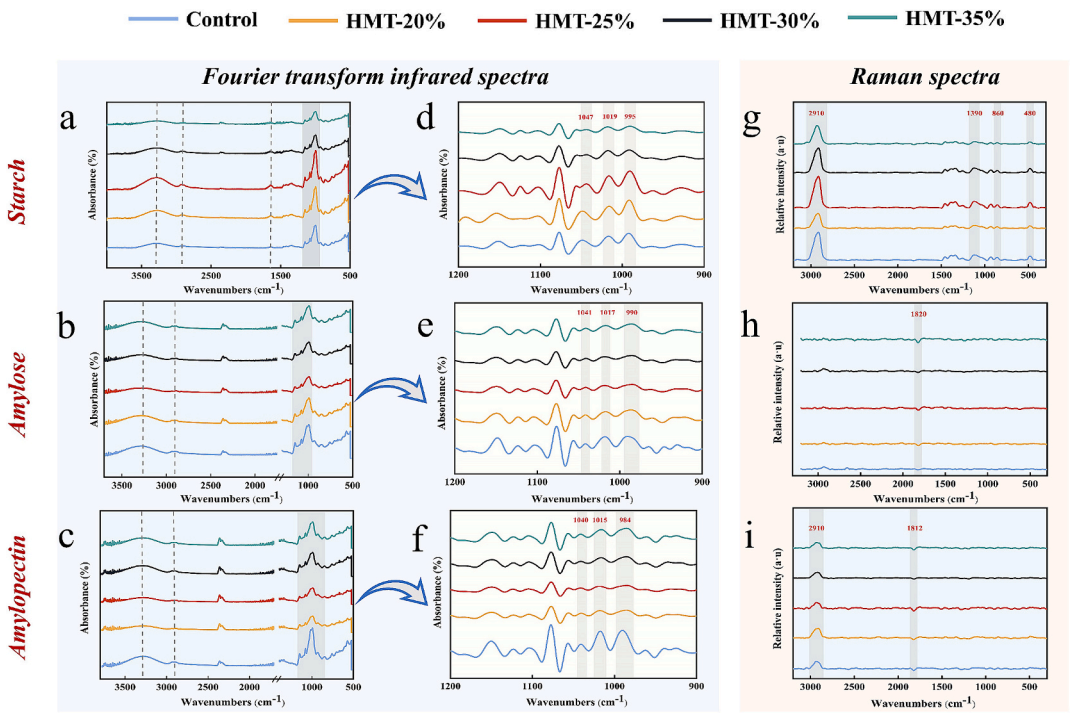


**Fig. 4.** FTIR and Raman spectra of starch, amylose and amylopectin modified by HMT. (a-c) FTIR spectra of starch, amylose and amylopectin. (d-f) Deconvoluted spectra (1200–900 $cm^{-1}$) of starch, amylose and amylopectin. (g-i) Raman spectra of starch, amylose and amylopectin.

structures. The infrared absorption peaks in the range of 3700–3000 $cm^{-1}$ are attributed to O—H stretching vibrations (Sevenou, Hill, Farhat, & Mitchell, 2002). These peaks encompass both free hydroxyl groups and hydroxyl groups bound to water molecules in crystalline or amorphous regions. Peak intensity increased at 20 % and 25 % MC, potentially due to enhanced interactions between starch molecules and increased hydrogen bonding (Chung, Lim, & Lim, 2006). As MC increased, starch tended towards a glassy state. Hydrogen bonds stabilizing the double helical structure were disrupted and bound by free ends that did not form double helical chains (Zhong et al., 2023), resulting in decreased peak strength for HMT-30 % and HMT-35 % starches. The band at 2920–2930 $cm^{-1}$, corresponding to asymmetric C—H bond vibrations, weakened with increased MC, possibly due to glycosidic bond breakage, corroborating the XRD results (Wang et al., 2022). The weak band at 1640 $cm^{-1}$ could be attributed to C—O or C—C group stretching vibrations (Gao et al., 2021). Bands at 1200–900 $cm^{-1}$ correlate to C—O stretching within the C-O-H moiety and C-O-C vibrations of the main chain. As shown in Fig. 4d, the peak at 995 $cm^{-1}$ may be linked to hydrogen bonding between hydroxyl groups at the $C_6$ position of the reactive glucose ring (Sun et al., 2021). As reported in Table 1, HMT-modified starch exhibited a significant increase in degree of DD values, possibly due to the re-formation of hydrogen bonds and new double helix rearrangement. Conversely, the DO values showed a decreasing trend. These findings suggest that HMT promoted the formation of new double helices in the amorphous phase, improving the physical characteristics and enzymatic resistance of starch granules.

Fig. 4b and c depict the FTIR spectra of amylose and amylopectin, respectively. Both components retained O—H, C—H, and C—O groups compared to starch. In the 3700–3000 $cm^{-1}$ range, peak intensities of HMT-modified amylose and amylopectin were slightly lower than the control, indicating disrupted hydrogen bonding (Chung et al., 2006). Further analysis of characteristic peaks at 1200–900 $cm^{-1}$ (Fig. 4e and f) revealed that amylose DD and DO values (Table 1) increased with MC. HMT treatment enhanced amylose orderliness, promoting chain movements and double helix structure formation in amorphous regions (Guo et al., 2020). Amylopectin DD and DO values (Table 1) initially increased and then decreased with increased MC compared to the control. This trend may be attributed to slight HMT treatment enhancing amylopectin hydrogen bonding and crystallinity in the amorphous region. Conversely, excess water molecules, driven by thermal action, disrupted hydrogen bonding and molecular ordering (Varatharajan, Hoover, Liu, & Seetharaman, 2010). In conclusion, the rearrangement of the starch double helix structure appears to be closely linked to amylose in the amorphous region, resembling the theory underlying starch double helix formation in lotus seed as studied by Chen et al. (2019).

### 3.4.2. *Raman spectra*

FTIR mainly resolves the backbone vibrations of α-(1,4) glycosidic bonds, whereas Raman spectra are more sensitive to the overall backbone vibrational modes (Lu et al., 2023). The Raman spectrum of starch, amylose and amylopectin were presented in Fig. 4g-i. The distinctive peak at 860 $cm^{-1}$ was correlated to the $C_1$-O-$C_4$ groups of the glucose ring, which were aligned along the axis of the double helix structure of amylose (Zheng et al., 2021). 1390 $cm^{-1}$ was attributed to a shift in the C-O-H bond angle, which was the result of recrystallization of single-helixed amylose (Z. Guo et al., 2019). The 3000–2800 $cm^{-1}$ Raman bands could evaluate the C—H bonds that were altered by the double helix of the formed amylopectin (Zheng, Tian, et al., 2021). The assessment of the short-range molecular order in starch using the FWHM of the Raman bands has become a common tool. Higher FWHM values in the Raman band indicated lower RC. As presented in Table 1, the FWHM values at 865 $cm^{-1}$, 1343 $cm^{-1}$, 2910 $cm^{-1}$ were decreased compared to the control. This indicated that the double helix of amylose, single helix of amylose and double helix of amylopectin were arranged in an increased order. On the other hand, the increase in FWHM at 480 $cm^{-1}$ verified the decrease in RC with the increase in DD. It also demonstrated that the molecules in the basic vibrational state directly absorb thermal energy, while the addition of excess water molecules led to the disruption and rearrangement of intramolecular and intermolecular hydrogen bonding (Fan et al., 2012). Moreover, random, disordered, unbound starch chains in the system formed a new double helix structure through hydrogen bonding, and the chemical groups achieved a new steady state

**Table 1**
FTIR parameters, FWHM, Fine structural, Pasting parameters and DSC parameters of HMT starch. Different lowercase letters (a-e) indicate significant differences ($p < 0.05$) in the mean values within the same. Parameter group.

| | Control | HMT-20 % | HMT-25 % | HMT-30 % | HMT-35 % |
|---|---|---|---|---|---|
| FTIR parameters | | | | | |
| DO (Starch) | 0.58 ± 0.011$^{b}$ | 0.62 ± 0.002$^{a}$ | 0.54 ± 0.003$^{c}$ | 0.47 ± 0.003$^{d}$ | 0.48 ± 0.003$^{d}$ |
| DO (AM) | 0.50 ± 0.002$^{d}$ | 0.61 ± 0.004$^{c}$ | 0.63 ± 0.001$^{b}$ | 0.63 ± 0.003$^{b}$ | 0.64 ± 0.004$^{a}$ |
| DO (AP) | 0.38 ± 0.002$^{d}$ | 0.53 ± 0.004$^{b}$ | 0.63 ± 0.005$^{a}$ | 0.53 ± 0.005$^{b}$ | 0.51 ± 0.006$^{c}$ |
| DD (Starch) | 1.28 ± 0.002$^{d}$ | 1.30 ± 0.003$^{c}$ | 1.31 ± 0.003$^{b}$ | 1.34 ± 0.003$^{a}$ | 1.34 ± 0.004$^{a}$ |
| DD (AM) | 1.03 ± 0.015$^{d}$ | 1.21 ± 0.025$^{c}$ | 1.22 ± 0.003$^{bc}$ | 1.22 ± 0.004$^{a}$ | 1.23 ± 0.003$^{a}$ |
| DD (AP) | 1.02 ± 0.015$^{d}$ | 1.09 ± 0.012$^{c}$ | 1.18 ± 0.002$^{a}$ | 1.13 ± 0.002$^{b}$ | 1.11 ± 0.003$^{bc}$ |
| Raman-FWHM | | | | | |
| $Starch_{2910}$ | 94.64 ± 0.37$^{a}$ | 91.50 ± 0.23$^{d}$ | 94.35 ± 0.35$^{a}$ | 93.35 ± 0.19$^{b}$ | 92.45 ± 0.38$^{c}$ |
| $Starch_{1343}$ | 101.65 ± 0.37$^{b}$ | 94.60 ± 0.32$^{c}$ | 105.76 ± 0.17$^{a}$ | 101.42 ± 0.30$^{b}$ | 74.59 ± 0.46$^{d}$ |
| $Starch_{865}$ | 41.64 ± 0.35$^{a}$ | 37.56 ± 0.34$^{c}$ | 40.44 ± 0.29$^{b}$ | 40.43 ± 0.47$^{b}$ | 36.47 ± 0.17$^{d}$ |
| $Starch_{480}$ | 46.23 ± 0.12$^{d}$ | 46.83 ± 0.19$^{c}$ | 47.68 ± 0.37$^{ab}$ | 47.44 ± 0.19$^{b}$ | 47.70 ± 0.41$^{a}$ |
| Fine structural parameters | | | | | |
| $h_{AP2}/h_{AP1}$ | 0.4457 ± 0.001$^{c}$ | 0.4442 ± 0.001$^{b}$ | 0.4456 ± 0.002$^{b}$ | 0.4461 ± 0.001$^{a}$ | 0.4463 ± 0.001$^{a}$ |
| $h_{AM}/h_{AP1}$ | 0.1271 ± 0.001$^{a}$ | 0.1103 ± 0.002$^{b}$ | 0.1053 ± 0.001$^{c}$ | 0.0958 ± 0.001$^{d}$ | 0.0855 ± 0.002$^{e}$ |
| Pasting parameters | | | | | |
| PV (cp) | 1327 ± 24.18$^{b}$ | 1403 ± 16.33$^{a}$ | 1239 ± 14.75$^{b}$ | 564 ± 41.21$^{c}$ | 324 ± 31.05$^{d}$ |
| TV (cp) | 1204 ± 11.21$^{b}$ | 1271 ± 21.42$^{a}$ | 1134 ± 12.11$^{c}$ | 509 ± 31.60$^{d}$ | 276 ± 29.18$^{e}$ |
| BD (cp) | 123 ± 12.97$^{ab}$ | 132 ± 5.09$^{a}$ | 105 ± 2.64$^{c}$ | 55 ± 9.61$^{d}$ | 48 ± 1.87$^{d}$ |
| SV (cp) | 1394 ± 15.51$^{b}$ | 1492 ± 17.43$^{a}$ | 1230 ± 12.69$^{c}$ | 573 ± 30.11$^{d}$ | 341 ± 28.62$^{e}$ |
| SB (cp) | 190 ± 4.3$^{b}$ | 222 ± 3.99$^{a}$ | 96 ± 0.58$^{c}$ | 64 ± 1.49$^{d}$ | 65 ± 0.56$^{e}$ |
| DSC parameters | | | | | |
| To (°C) | 58.82 ± 0.04$^{d}$ | 61.6 ± 0.92$^{c}$ | 64.19 ± 0.01$^{b}$ | 66.05 ± 0.13$^{a}$ | 66.09 ± 0.01$^{a}$ |
| Tp (°C) | 64.08 ± 0.01$^{e}$ | 67.70 ± 0.01$^{d}$ | 69.57 ± 0.01$^{c}$ | 70.83 ± 0.05$^{b}$ | 71.12 ± 0.03$^{a}$ |
| Tc (°C) | 72.58 ± 0.20$^{e}$ | 76.30 ± 0.12$^{d}$ | 78.32 ± 0.10$^{c}$ | 79.66 ± 0.41$^{b}$ | 80.72 ± 0.58$^{a}$ |
| ΔH (J/g) | 1.81 ± 0.04$^{a}$ | 1.67 ± 0.05$^{b}$ | 1.14 ± 0.04$^{c}$ | 0.92 ± 0.01$^{d}$ | 0.90 ± 0.07$^{d}$ |

(Lu et al., 2023). No characteristic peaks similar to starch were measured for amylose and amylopectin. The presence of a characteristic peak at 1800 $cm^{-1}$ was not captured in previous studies and warranted further exploration. As a result, Raman spectra might not be able to account for the relationship between starch-amylose- amylopectin.

### 3.5. Chain length distribution

The SEC weight chain length distributions (CLDs) as a function of degree of polymerization (DP) (X), w log (X), for starch modified by HMT are presented in Fig. 5a. All samples exhibited similar chain length distributions, consistent with previous studies (Ahmed et al., 2019). The distributions comprised three distinct regions: (i) The primary amylopectin peak ($AP_1$), corresponding to chains confined within single crystalline/amorphous lamellae, predominantly consisting of short-chain amylopectin. (ii) A shoulder peak ($AP_2$), correlating to chains spanning two or more crystalline lamellae, encompassing medium and long chains of amylopectin and short-chained amylose. (iii) The lowest peak, reflecting the medium-long chains of amylose. Although the peak positions of $AP_1$ and $AP_2$ remained relatively constant across samples, a significant difference in the $h_{AP2}/h_{AP1}$ ratio was observed, indicating an increase in medium and long chains of amylopectin. Concurrently, the $hAM/hAP_1$ ratio exhibited a decreasing trend, suggesting the degradation of amylose into shorter or medium chains. This observation aligns with Lan et al. (2008), who attributed the decrease in rectilinear amylose content of hydrothermally treated starch to alterations in the structural conformation of amylose, explaining the reduced peak intensity in the amylose region.

Following the classification proposed by (Ahmed et al., 2019), branched chains were categorized as A chain (DP 6–12), $B_1$ chain (DP 13–24), $B_2$ chain (DP 25–36), and $B_{3+}$ chain (DP > 36), representing short, medium, long, and very long chains, respectively. As illustrated in Fig. 5b-f, the proportion of A chain demonstrated a decreasing trend with increasing MC. This phenomenon can be attributed to molecular disruption occurring predominantly in the outer branches of amylopectin. HMT was found to cleave α-(1,6) linkages, resulting in the dislodgement of A chain. Furthermore, the reduction in A chain was correlated with a decrease in RC. Notably, the proportion of longer chains remained unaffected by HMT, likely due to their crystalline state rendering them more resistant to thermal degradation. The observed increase in the proportion of $B_1$ chain could be attributed to partial fragmentation of $B_2$ and $B_{3+}$ chain lengths, a finding consistent with the study conducted by Bian and Chung (2016). In conjunction with XRD and Fourier-transform infrared spectroscopy (FTIR) analyses, it is hypothesized that the detachment of amylopectin short chains exerts an inhibitory effect on amylose reorganization.

### 3.6. Physicochemical properties of starch

#### 3.6.1. Solubility and SP

The solubility and SP of starch were plotted in Fig. 6a. The HMT-modified starch exhibited greater solubility than the natural starch at 25 °C and 100 °C compared to the control. The maximum solubility increased by 720.93 % (25 °C) and 92.32 % (100 °C), respectively. This could be attributed to the leaching of short-chain starch, which was caused by hydrogen bond breaking and debranching amylopectin. The solubility of wheat starch was inhibited by steam modification according to Ma et al. (2021). This was due to partial pasting which prompted the degradation chains to inhibit their leaching through non-covalent recombination. This might in turn mean that in the present study, the starch was modified to produce more free starch chains. It was closely related to the decrease in RC of both starch and amylose. For SP, the opposite trend was observed at 25 °C and 100 °C. The SP increased by 152.94 % at 25 °C, while it decreased by 34.94 % at 100 °C. It was more dependent on the disruption of the amorphous region, and the exposure of hydrophilic hydroxyl groups led to an increase in SP at 25 °C (Li & Zhu, 2017). Additionally, the increase in short chains led to defective crystal structures, which favored water penetration and led to an increase in SP. Similarly, the decrease in the percentage of short chains increased the mobility of amylopectin, increasing the possibility of entanglement of apparent amylose with it during the cooling phase of HMT, and therefore SP was suppressed at 100 °C (Q. Wang et al., 2022).

#### 3.6.2. Pasting property

Pasting viscosity properties, which reflect gelatinization, disintegration, swelling, and gel-forming abilities, are crucial characteristics for the selection of industrial starch resources. The pasting characteristics of the starch, as determined by RVA, are presented in Fig. 6b. Following HMT, the overall viscosity values of the starch exhibited a decreasing trend. The PV (1403 cp) and TV (1271 cp) of HMT-20 % starch were observed to be higher than the control. However, with increasing MC, the PV demonstrated a decreasing trend. This phenomenon may be attributed to the highly dense structure of starch at low MC, resulting in more intense collisions and friction between starch chains, as suggested by Gong et al. (2017). As MC increased, the breakage of hydrogen and glycosidic bonds accelerated, leading to improved

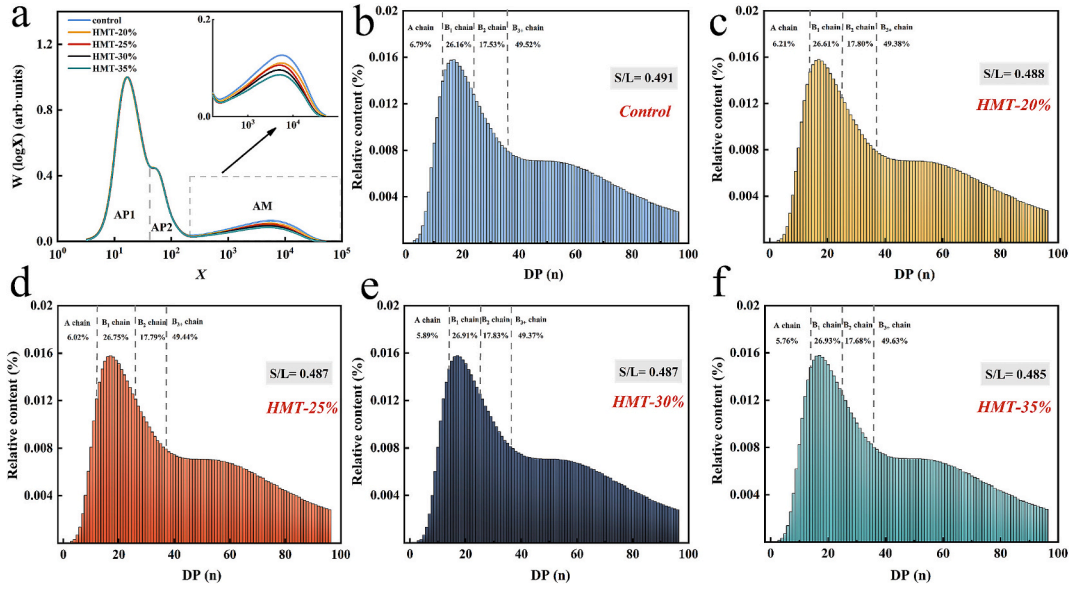


**Fig. 5.** The chain length information of starch modified by HMT. (a) SEC weight chain-length distributions (CLDs). (b-f) Chain length distribution of starch modified by HMT. S/L was the ratio of relative content of short chains (A + $B_1$) to that of long chains ($B_2$ + $B_{3+}$).

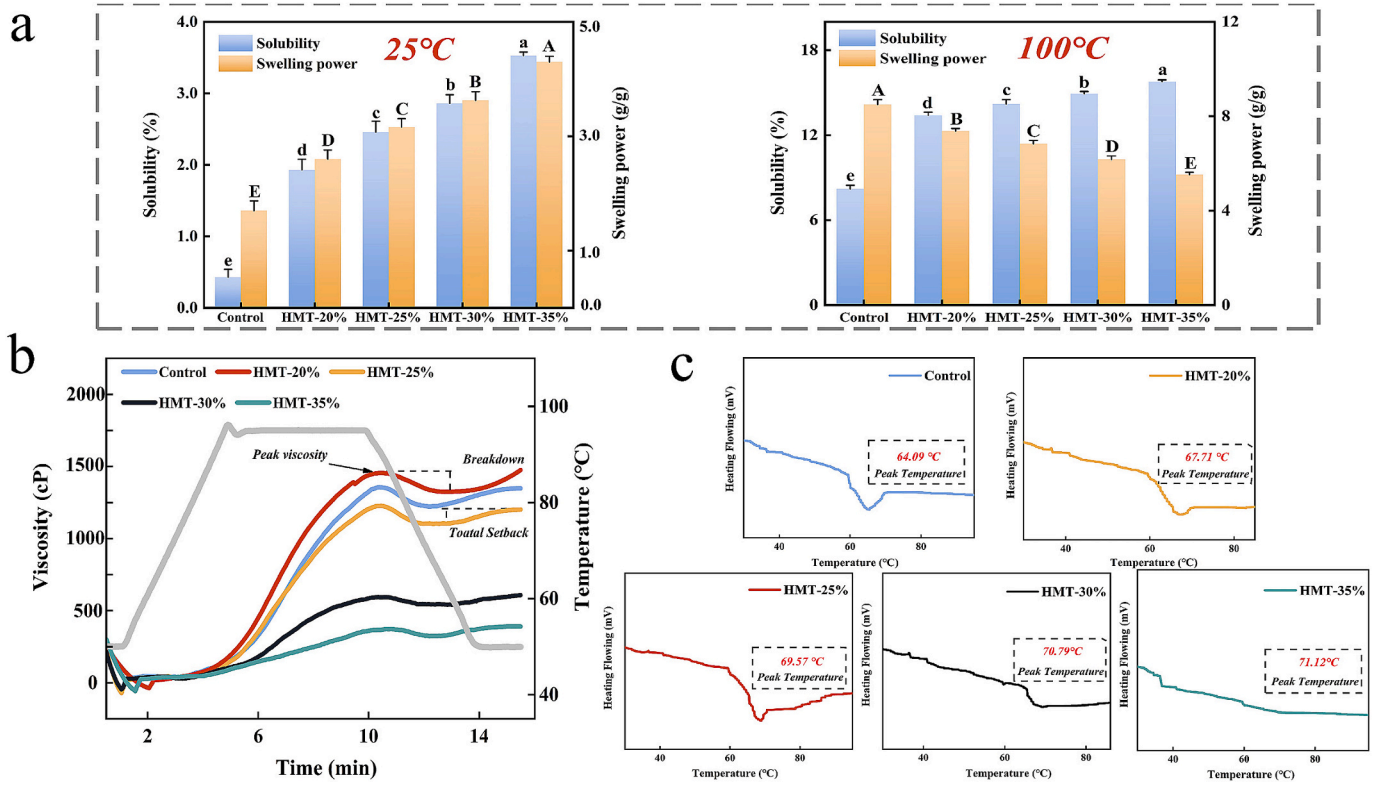


**Fig. 6.** Changes of solubility and swelling power (a), pasting properties (b) and thermal property (c) of starch with HMT. Different capitals and lowercase letters (a-e) indicate significant differences ($p$<0.05) in the mean values within the same parameter group.

freedom of amylose in the amorphous region. This enhancement in recrystallization ability was accompanied by weakened interactions with water molecules, ultimately resulting in decreased viscosity, as reported by Huang, Zhou, Jin, Xu, and Chen (2016). The TV, representing the lowest viscosity at the conclusion of the heating phase, decreased to a minimum of 276 cp with increasing MC. This reduction is likely due to the increased flexibility of long amylose chains, which accelerated the formation of dextran chain complexes and decreased particle size, as observed by Sharma, Singh, and Subramanian (2013). Upon completion of the cooling phase, a cold paste was formed. The decrease in FV can be attributed to the reduced number of free amylose molecules, which diminished chain interactions. The difference between FV and TV provides insight into the starch's tendency for retrogradation. This property has potential applications in modifying the cooking time and softness of pasta, demonstrating significant practical value in food processing.

### 3.6.3. Thermal property

The thermal characterization transition parameters of starch modified by HMT, which include *To* (onset temperature), $T_p$ (peak temperature), *Tc* (conclusion temperature) and $\Delta H$ (gelatinization enthalpy), are presented in Table 1 and Fig. 6c. Gelatinization of starch was initiated at 58.82 °C, the *To*, *Tp* and *Tc* of starch improved significantly with the increased MC, indicating that HMT promoted the thermal stability of starch. This could be caused by the movement of short chains from the amorphous region to the crystalline region, which participated in the formation of double helix to form a dense structure. ΔH could be used to evaluate the crystallinity, which was an indicator of the order loss of starch molecular chains in the crystalline region. In addition, the crystal linearity indicated the stability of the ordered structure arrangement of the starch molecular chain and the proportion of the crystalline region (He et al., 2021). In contrast, the ΔH of HMT-treated starch decreased from 1.81 J/g to 0.90 J/g. This revealed that HMT led to partial loss of crystallization, stimulating unraveling and disordering of the amylose double helix, with the short chains becoming an obstacle to the recombination of adjacent long chains, leading to decreased ΔH (Gong et al., 2017). This was the same thermal stability result obtained with HMT-treated sweet potato starch by Sun, Qin, Zeng, and Li (2023).

### 3.6.4. Rheological property

The steady-state shear and dynamic rheological profiles of HMT-modified starch are illustrated in Fig. 7. As shown in Fig. 7a, all starch samples exhibited non-Newtonian shear thinning behavior, with apparent viscosity decreasing as shear rate increased. During HMT processing, the fluidity was modified with increasing MC. Amylose, being the primary component of the amorphous region, experienced an increase in its degree of ordering, leading to an enhancement of the starch's rigid structure. This enhancement subsequently disrupted the organized crystal structure, as confirmed by FTIR and XRD analyses. The storage modulus (G′) was closely related to the angular frequency and represented the elastic properties, while the loss modulus (G″) denoted the viscous properties (Zhong et al., 2023). As depicted in Figs. 7b and c, the G′ values consistently exceeded G″, indicating that all starches exhibited good elasticity. This revealed a slight enhancement in the elastic behavior of HMT-20 % and HMT-25 % starches, which could be attributed to the interaction and aggregation of amylose in the early stage, as evidenced by XRD analysis. The dissociation and leaching of small molecular chains of amylose were identified as the underlying cause for the decrease in G′ as MC continued to increase (Gao et al., 2021). It was observed that low moisture content may be insufficient to induce starch gelatinization transition at high temperatures, while higher moisture content can lead to the precipitation of a large amount of irreversible starch. The recrystallization of small-chained starch reduced the aggregation of free chains. Fig. 7d demonstrated that all samples exhibited better pseudoplasticity, with tan δ values less than 1. The tan δ of HMT-treated samples was lower than that of the control group, indicating that HMT treatment increased the hardness of the samples. These findings suggest potential applications in food products such as cold cuts and porridge.

### 3.7. In vitro digestibility

Starch is categorized as rapid-digesting starch (RDS), slow-digesting starch (SDS), and resistant starch (RS) based on the speed at which the body absorbs and digests the starch. When treated with HMT-40 %, RDS and SDS decreased by 25.36 % and 8.44 %, respectively, while RS increased by 85.26 % compared to the control, as shown in Fig. 8a. To further clarify the resistance of starch to the enzyme, the hydrolysis rates of HMT-treated starches were compared (Fig. 8b). The samples were all rapidly digested within 40 min, while the growth was slower from 60 to 180 min. The digestion rate of starch gradually decreased with increased MC. Huang et al. (2016) demonstrated that HMT treatment reduced the RDS of brown rice starch and significantly increased the RS. In the first-order model, LOS predicted the hydrolysis of starch. The digestibility (K) represented the reaction rate of starch hydrolysis. The values of K from control to HMT-40 % were 0.35, 0.34, 0.32, 0.32, and 0.31, respectively, which indicated that the digestion rate was slowest when the MC was 40 %, in keeping with the data we obtained. Jane, Wong, and McPherson (1997) showed that in A-type starches, branching points were

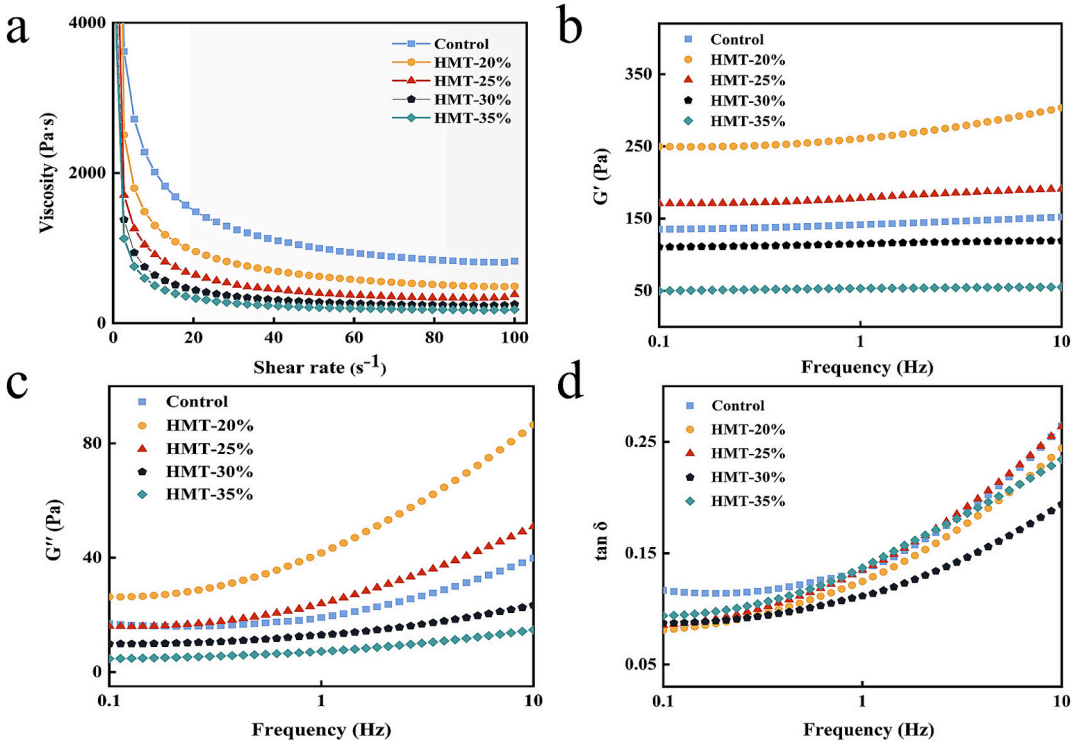


**Fig. 7.** Rheological properties of rice starch with HMT. (a) The apparent viscosity, (b) the elastic modulus (G′), (c) loss modulus (G″), (d) the loss angle (tanδ).

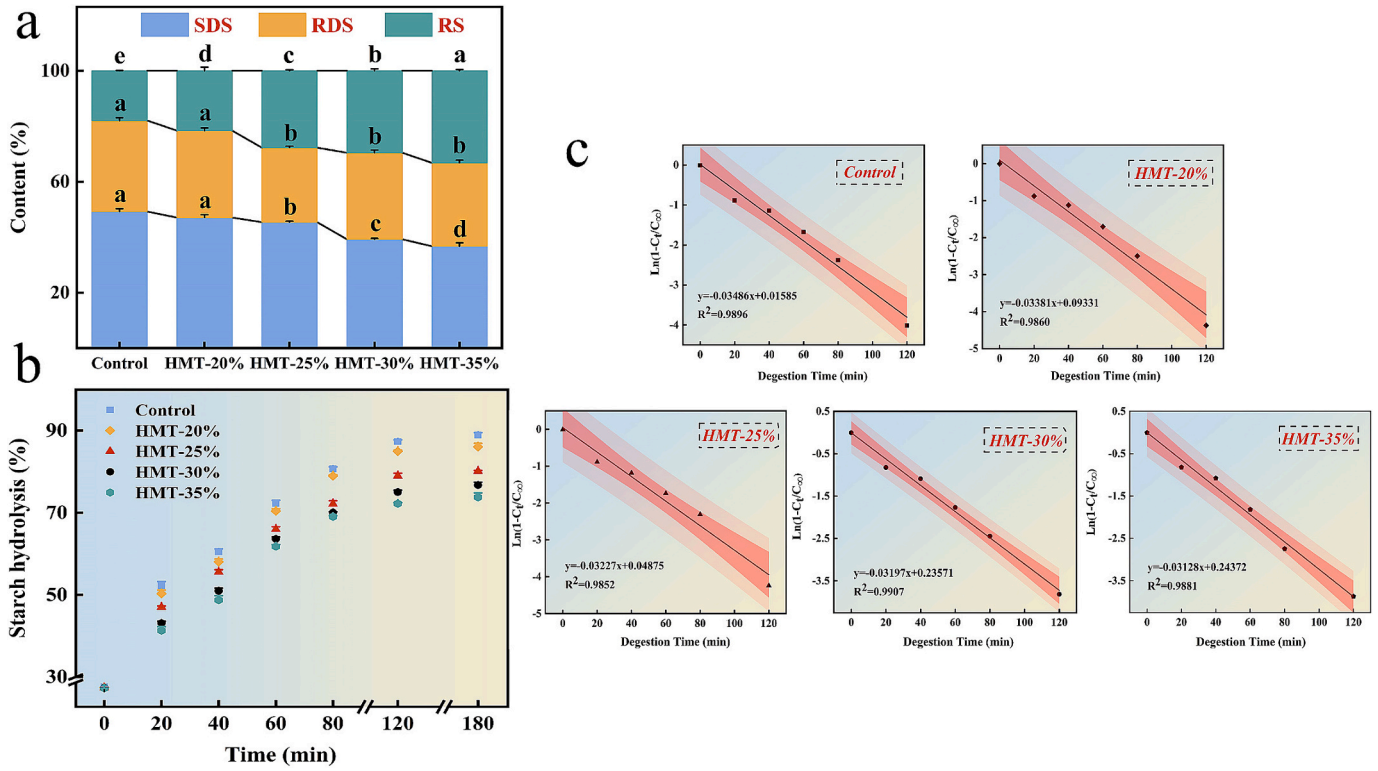


**Fig. 8.** In vitro digestive properties of rice starch with HMT. (a) The digested starch content, (b) the rate of starch hydrolysis, (c) the first-order kinetic fitting equation. Different lowercase letters (a-e) indicate significant differences ($p<0.05$) in the mean values within the same parameter group.

distributed in both the amorphous and crystalline regions, so that there were more short chains derived from branched chains in the crystalline region, resulting in more sites of hydrolytic action by α-amylase. Based on the results of chain length distribution, it was reasonable that the reduction of the A chain was used to confirm the decrease in the enzymatic hydrolysis rate. In addition, the rearrangement of the double helix structure led to the dense structure of the amorphous region, reducing the hydrolysis sites of α-amylase and decreasing its sensitivity. Hence, the decrease in digestion rate and the increase in resistant starch were attributed to the disorganization and reorganization of amylose induced by HMT, whereby the amorphous regions became denser and the sensitivity of the starch to enzymes was diminished (Wang et al., 2016). This promoted the conversion of RDS to RS and a decrease in the digestion rate. Accordingly, the effect of HMT on starch digestibility was achieved by regulating the structural disorder and recrystallization of amylose.

## 4. Conclusions

This study investigated the structural changes in starch, amylose, and amylopectin during HMT while also elucidating the relationship between physicochemical characteristics and structure. As MC increased, starch exhibited signs of gelatinization, with amylose displaying a more pronounced molten state compared to amylopectin. The decrease in crystallinity of starch indicated disruption of its crystalline region and rearrangement of the amorphous region. Amylose demonstrated structural evolution, while the degradation of short-chain amylopectin hindered amylose rearrangement. Consequently, amylose exhibited a strong recrystallization tendency, forming a dense structure that played a dominant role in determining the physicochemical characteristics of starch. Solubility and thermal stability increased with higher MC, while viscosity and viscoelasticity were enhanced by moderate moisture levels. The resistance of the starch substrate to enzymatic digestion gradually increased. These properties can be regulated by varying the MC during HMT. The findings of this study contribute to a better understanding of the relationship between the structures of amylose, amylopectin, and starch from a structural perspective. This knowledge provides a foundation for the rational design of functional starch-based foods using HMT.

## CRediT authorship contribution statement

**Weijie Qi:** Writing – review & editing, Writing – original draft, Methodology, Data curation, Conceptualization. **Siying Kong:** Investigation, Data curation. **Xiaoqiang Li:** Investigation, Formal analysis. **Zeyu Peng:** Conceptualization. **Lina Sun:** Funding acquisition. **Zhaohua Wang:** Writing – review & editing. **Jianjun Cheng:** Writing – review & editing, Supervision, Methodology, Formal analysis.

## Declaration of competing interest

The authors declare that they have no known competing financial interests or personal relationships that could have appeared to influence the work reported in this paper.

## Acknowledgment

This work was supported by National Natural Science Foundation of China (grant numbers 32372253).

## Appendix A. Supplementary data

Supplementary data to this article can be found online at https://doi.org/10.1016/j.fochx.2024.101942.

## Data availability

Data will be made available on request.

## References


Ahmed, S., Ru, W., Han, H., Cheng, L., Bian, X., Li, G., & Bao, J. (2019). Fine molecular structure and its effects on physicochemical properties of starches in potatoes grown in two locations. *Food Hydrocolloids, 97*, Article 105172. https://doi.org/10.1016/j.foodhyd.2019.105172

Ang, C. L., Goh, K. K. T., Lim, K., & Matia-Merino, L. (2021). Rheological characterization of a physically-modified waxy potato starch: Investigation of its shear-thickening mechanism. *Food Hydrocolloids, 120*, Article 106908. https://doi.org/10.1016/j.foodhyd.2021.106908

Bertoft, E., Koch, K., & Åman, P. (2016). Structure of clusters and building blocks in amylopectin from African rice accessions. *Carbohydrate Polymers, 361*, 105–113. https://doi.org/10.1016/j.carbpol.2016.04.057

Bian, L., & Chung, H.-J. (2016). Molecular structure and physicochemical properties of starch isolated from hydrothermally treated brown rice flour. *Food Hydrocolloids, 60*, 345–352. https://doi.org/10.1016/j.foodhyd.2016.04.008

Chen, C., Fu, W., Chang, Q., Zheng, B., Zhang, Y., & Zeng, H. (2019). Moisture distribution model describes the effect of water content on the structural properties of lotus seed resistant starch. *Food Chemistry, 286*, 449–458. https://doi.org/10.1016/j.foodchem.2019.01.214

Chung, H.-J., Lim, H. S., & Lim, S.-T. (2006). Effect of partial gelatinization and retrogradation on the enzymatic digestion of waxy rice starch. *Journal of Cereal Science, 43*(3), 353–359. https://doi.org/10.1016/j.jcs.2005.12.001

Fan, D., Ma, W., Wang, L., Huang, J., Zhao, J., Zhang, H., & Chen, W. (2012). Determination of structural changes in microwaved rice starch using Fourier transform infrared and Raman spectroscopy. *Starch-Stärke, 64*(8), 598–606. https://doi.org/10.1002/star.201100200

Gao, S., Liu, H., Sun, L., Cao, J., Yang, J., Lu, M., & Wang, M. (2021). Rheological, thermal and in vitro digestibility properties on complex of plasma modified Tartary buckwheat starches with quercetin. *Food Hydrocolloids, 110*, Article 106209. https://doi.org/10.1016/j.foodhyd.2020.106209

Gong, B., Xu, M., Li, B., Wu, H., Liu, Y., Zhang, G., & Li, W. (2017). Repeated heat-moisture treatment exhibits superiorities in modification of structural, physicochemical and digestibility properties of red adzuki bean starch compared to continuous heat-moisture way. *Food Research International, 102*, 776–784. https://doi.org/10.1016/j.foodres.2017.09.078

Guo, B., Wang, Y., Pang, M., Wu, J., Hu, X., Huang, Z., & Liu, C. (2020). Annealing treatment of amylose and amylopectin extracted from rice starch. *International Journal of Biological Macromolecules, 164*, 3496–3500. https://doi.org/10.1016/j.ijbiomac.2020.08.245

Guo, Z., Jia, X., Lin, X., Chen, B., Sun, S., & Zheng, B. (2019). Insight into the formation, structure and digestibility of lotus seed amylose-fatty acid complexes prepared by high hydrostatic pressure. *Food and Chemical Toxicology, 128*, 81–88. https://doi.org/10.1016/j.fct.2019.03.052

He, Y., Chen, F., Shi, Y., Guan, Z., Zhang, N., & Campanella, O. H. (2021). Physico-chemical properties and structure of rice cultivars grown in Heilongjiang province of China. *Food Science and Human Wellness, 10*(1), 45–53. https://doi.org/10.1016/j.fshw.2020.05.010

Hizukuri, S. (1986). Polymodal distribution of the chain lengths of amylopectins, and its significance. *Carbohydrate Research, 147*(2), 342–347. https://doi.org/10.1016/S0008-6215(00)90643-8

Huang, T.-T., Zhou, D.-N., Jin, Z.-Y., Xu, X.-M., & Chen, H.-Q. (2016). Effect of repeated heat-moisture treatments on digestibility, physicochemical and structural properties of sweet potato starch. *Food Hydrocolloids, 54*, 202–210. https://doi.org/10.1016/j.foodhyd.2015.10.002

Jane, J. L., Wong, K. S., & McPherson, A. E. (1997). Branch-structure difference in starches of A-and B-type X-ray patterns revealed by their Naegeli dextrins. *Carbohydrate Research, 300*(3), 219–227. https://doi.org/10.1016/s0008-6215(97)00056-6

Kumar, S. R., Tangsrianugul, N., Sriprablom, J., Wongsagonsup, R., Wansuksri, R., & Suphantharika, M. (2023). Effect of heat-moisture treatment on the physicochemical properties and digestibility of proso millet flour and starch. *Carbohydrate Polymers, 307*, Article 120630. https://doi.org/10.1016/j.carbpol.2023.120630

Lan, H., Hoover, R., Jayakody, L., Liu, Q., Donner, E., Baga, M., & Chibbar, R. (2008). Impact of annealing on the molecular structure and physicochemical properties of normal, waxy and high amylose bread wheat starches. *Food Chemistry, 111*(3), 663–675. https://doi.org/10.1016/j.foodchem.2008.04.055

Li, G., & Zhu, F. (2017). Amylopectin molecular structure in relation to physicochemical properties of quinoa starch. *Carbohydrate Polymers, 164*, 396–402. https://doi.org/10.1016/j.carbpol.2017.02.014

Lopez-Rubio, A., Flanagan, B. M., Gilbert, E. P., & Gidley, M. J. (2010). A novel approach for calculating starch crystallinity and its correlation with double helix content: A combined XRD and NMR study. *Biopolymers, 89*(9), 761–768. https://doi.org/10.1002/bip.21005

Lu, H., Tian, Y., & Ma, R. (2023). Assessment of order of helical structures of retrograded starch by Raman spectroscopy. *Food Hydrocolloids, 134*, Article 108064. https://doi.org/10.1016/j.foodhyd.2022.108064

Ma, Y., Zhang, W., Pan, Y., Ali, B., Xu, D., & Xu, X. (2021). Physicochemical, crystalline characterization and digestibility of wheat starch under superheated steam treatment. *Food Hydrocolloids, 118*, Article 106720. https://doi.org/10.1016/j.foodhyd.2021.106720

Schafranski, K., Ito, V. C., & Lacerda, L. G. (2021). Impacts and potential applications: A review of the modification of starches by heat-moisture treatment (HMT). *Food Hydrocolloids, 117*, Article 106690. https://doi.org/10.1016/j.foodhyd.2021.106690

Sevenou, O., Hill, S., Farhat, I., & Mitchell, J. (2002). Organisation of the external region of the starch granule as determined by infrared spectroscopy. *International Journal of Biological Macromolecules, 31*(1–3), 79–85. https://doi.org/10.1016/s0141-8130(02)00067-3

Sharma, P., Singh, V., & Subramanian, R. (2013). Pasting, swelling, and solubility characteristics of rice batter prepared from different wet grinding systems. *Starch-Stärke, 65*(5–6), 374–381. https://doi.org/10.1002/star.201200126

Sun, X., Sun, Z., Saleh, A. S., Zhao, K., Ge, X., Shen, H., & Li, W. (2021). Understanding the granule, growth ring, blocklets, crystalline and molecular structure of normal and waxy wheat A-and B-starch granules. *Food Hydrocolloids, 121*, Article 107034. https://doi.org/10.1016/j.foodhyd.2021.107034

Sun, Y., Qin, R., Zeng, J., & Li, G. (2023). Effect of Heat–Moisture Treatment on the Structure and Digestibility of Sweet Potato Starch. *Foods, 12*(16), 3076. https://doi.org/10.3390/foods12163076

Tan X, T., Li, X., Chen, L., Xie, F., Li, L., & Huang, J. (2017). Effect of heat-moisture treatment on multi-scale structures and physicochemical properties of breadfruit starch. *Carbohydrate Polymers, 161*, 286–294. https://doi.org/10.1016/j.carbpol.2017.01.029

Tao, K., Li, C., Yu, W., Gilbert, R. G., & Li, E. (2019). How amylose molecular fine structure of rice starch affects functional properties. *Carbohydrate Polymers, 204*, 24–31. https://doi.org/10.1016/j.carbpol.2018.09.078

Vamadevan, V., & Bertoft, E. (2015). Structure-function relationships of starch components. *Starch-Stärke, 67*(1–2), 55–68. https://doi.org/10.1002/star.201400188

Varatharajan, V., Hoover, R., Liu, Q., & Seetharaman, K. (2010). The impact of heat-moisture treatment on the molecular structure and physicochemical properties of normal and waxy potato starches. *Carbohydrate Polymers, 81*(2), 466–475. https://doi.org/10.1016/j.carbpol.2010.03.002

Wang, H., Liu, Y., Chen, L., Li, X., Wang, J., & Xie, F. (2018). Insights into the multi-scale structure and digestibility of heat-moisture treated rice starch. *Food Chemistry, 242*, 323–329. https://doi.org/10.1016/j.foodchem.2017.09.014

Wang, H., Zhang, B., Chen, L., & Li, X. (2016). Understanding the structure and digestibility of heat-moisture treated starch. *International Journal of Biological Macromolecules, 88*, 1–8. https://doi.org/10.1016/j.ijbiomac.2016.03.046

Wang, Q., Li, L., Liu, C., & Zheng, X. (2022). Heat-moisture modified blue wheat starch: Physicochemical properties modulated by its multi-scale structure. *Food Chemistry, 386*, Article 132771. https://doi.org/10.1016/j.foodchem.2022.132771

Watcharatewinkul, Y., Puttanlek, C., Rungsardthong, V., & Uttapap, D. (2009). Pasting properties of a heat-moisture treated canna starch in relation to its structural characteristics. *Carbohydrate Polymers, 75*(3), 505–511. https://doi.org/10.1016/j.carbpol.2008.08.018

Yin, X., Zheng, Y., Kong, X., Cao, S., Chen, S., Liu, D., & Tian, J. (2021). RG-I pectin affects the physicochemical properties and digestibility of potato starch. *Food Hydrocolloids, 117*, Article 106687. https://doi.org/10.1016/j.foodhyd.2021.106687

Zheng, Y., Ou, Y., Zhang, C., Zhang, Y., Zheng, B., Zeng, S., & Zeng, H. (2021). The impact of various exogenous type starch on the structural properties and dispersion stability of autoclaved lotus seed starch. *International Journal of Biological Macromolecules, 175*, 49–57. https://doi.org/10.1016/j.ijbiomac.2021.01.175

Zheng, Y., Tian, J., Ogawa, Y., Yin, X., Xu, E., Chen, S., & Ye, X. (2021). Co-extrusion of proanthocyanins from Chinese bayberry leaves modifies the physicochemical properties as well as the in vitro digestion of restructured rice. *Food Structure, 27*, Article 100182. https://doi.org/10.1016/j.foostr.2021.100182

Zhong, Y., Tian, Y., Liu, X., Ding, L., & Blennow, A. (2021). Influence of microwave treatment on the structure and functionality of pure amylose and amylopectin systems. *Food Hydrocolloids, 119*(3), Article 106856. https://doi.org/10.1016/j.foodhyd.2021.106856

Zhong, Y., Yin, X., Yuan, Y., Kong, X., Chen, S., Ye, X., & Tian, J. (2023). Changes in physiochemical properties and in vitro digestion of corn starch prepared with heat-moisture treatment. *International Journal of Biological Macromolecules, 125912*. https://doi.org/10.1016/j.ijbiomac.2023.125912


## Further-reading


Chen, J., Chen, Y., Ge, H., Wu, C., Pang, J., & Miao, S. (2018). Multi-scale structure, pasting and digestibility of adlay (Coixlachryma-jobi L.) seed starch. *Food Hydrocolloids, 89*, 885–891. https://doi.org/10.1016/j.foodhyd.2018.11.050

Van Hung, P., Binh, V. T., Nhi, P. H. Y., & Phi, N. T. L. (2020). Effect of heat-moisture treatment of unpolished red rice on its starch properties and in vitro and in vivo digestibility. *International Journal of Biological Macromolecules, 154*, 1–8. https://doi.org/10.1016/j.ijbiomac.2020.03.071

Wang, D., He, Z., Yang, L., Wang, H., Lian, X., & Zhu, W. (2021). Retrogradation of sweet potato amylose and amylopectin with narrow molecular weight distribution. *International Journal of Food Science & Technology*. https://doi.org/10.1111/ijfs.15271